

# Isothermal Stimulation of Mineral Dissolution Processes by Acoustic Perturbation

Zongsu Wei,<sup>†,‡,§</sup> Yi-Hsuan Hsiao,<sup>†,‡,§</sup> Xin Chen,<sup>†</sup> Erika Callagon La Plante,<sup>†,§</sup> Iman Mehdipour,<sup>†</sup> Dante Simonetti,<sup>‡,§</sup> Narayanan Neithalath,<sup>§</sup> Laurent Pilon,<sup>||</sup> Mathieu Bauchy,<sup>⊥</sup> Jacob Israelachvili,<sup>#,∇</sup> and Gaurav Sant<sup>\*,†,⊙,◆</sup>

<sup>†</sup>Laboratory for the Chemistry of Construction Materials (LC<sup>2</sup>), Department of Civil and Environmental Engineering, University of California, Los Angeles, California 90095, United States

<sup>‡</sup>Department of Chemical and Biomolecular Engineering, University of California, Los Angeles, California 90095, United States

<sup>§</sup>School of Sustainable Engineering and the Built Environment, Arizona State University, Tempe, Arizona 85287, United States

<sup>||</sup>Department of Mechanical and Aerospace Engineering, University of California, Los Angeles, California 90095, United States

<sup>⊥</sup>Physics of Amorphous and Inorganic Solids Laboratory (PARISlab), Department of Civil and Environmental Engineering, University of California, Los Angeles, California 90095, United States

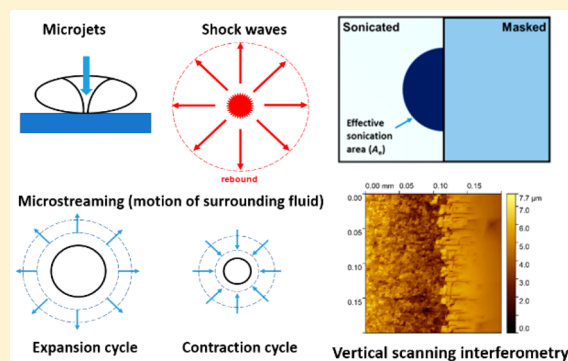
<sup>#</sup>Department of Chemical Engineering, University of California, Santa Barbara, California 93106, United States

<sup>∇</sup>California Nanosystems Institute (CNSI), University of California, Santa Barbara, California 93106, United States

<sup>⊙</sup>Department of Materials Science and Engineering, University of California, Los Angeles, California 90095, United States

<sup>◆</sup>California Nanosystems Institute (CNSI), University of California, Los Angeles, California 90095, United States

**ABSTRACT:** On the basis of systematic experimental interrogation of the aqueous dissolution behavior of a large selection of minerals, whose dissolution rates vary by several orders of magnitude, this study demonstrates that acoustic perturbation yields an unprecedented enhancement in dissolution kinetics, which scales with the mineral's hardness and average bond energy. The dissolution enhancement produced is described by an Arrhenius-like formulation that reveals the energy imparted to the solute's surficial atoms by sonication. From an energy landscape perspective, it is highlighted that sonication perturbs surficial solute atoms from their equilibrium positions. As a result, upon contact with a solvent, sonicated atoms need a smaller amount of energy for dissolution to occur by bond rupture. Therefore, the activation energy of dissolution under sonication is consistently smaller than that under sonication-free conditions. Altogether, this study suggests that the enhancement in mineral dissolution over the course of acoustic perturbation under macroscopically isothermal conditions results from the excitation of the surficial atoms and is negligibly associated with temperature rise or surface area amplification as has been previously suggested.



## 1. INTRODUCTION

The transmission of sonic stimuli into an aqueous solution can initiate the formation, growth, and collapse of cavitation bubbles.<sup>1,2</sup> Such cavitation can induce enormous energy changes in the form of “hot spots”.<sup>3</sup> The extremely high temperatures (up to 5000 K) and pressures (up to 1000 bar) that are generated (e.g., as typical for ultrasonication), locally, by sonication-induced cavitation offer pathways to expedite and control chemical reactions of relevance to element extraction, food engineering, and degradation of persistent pollutants.<sup>4,5</sup> For these reasons of efficient, localized treatment, and because it requires no chemical reagents, (ultra)sound is considered a “green” technology.<sup>6</sup>

The collapse of cavitation bubbles creates localized fluid movement with high pressure and velocity.<sup>7,8</sup> This includes

effects such as acoustic streaming, microstreaming, microjets, and shock waves (see Figure 1).<sup>9</sup> Specifically, acoustic streaming is defined as fluid flow due to ultrasonic propagation, whereas microstreaming refers to the oscillating motion of the fluid in the vicinity of expanding and contracting bubbles.<sup>7</sup> High-pressure shock waves (e.g., 1 MPa for 20 kHz waves)<sup>10</sup> are formed when a cavitation bubble collapses symmetrically. On the other hand, microjets (100–200 m/s in velocity)<sup>7</sup> result from the asymmetrical collapse of cavitation bubbles due to the presence of another surface or another bubble.<sup>11–14</sup> The generation of such extreme pressures and rapid fluid motion

**Received:** August 27, 2018

**Revised:** November 3, 2018

**Published:** November 26, 2018

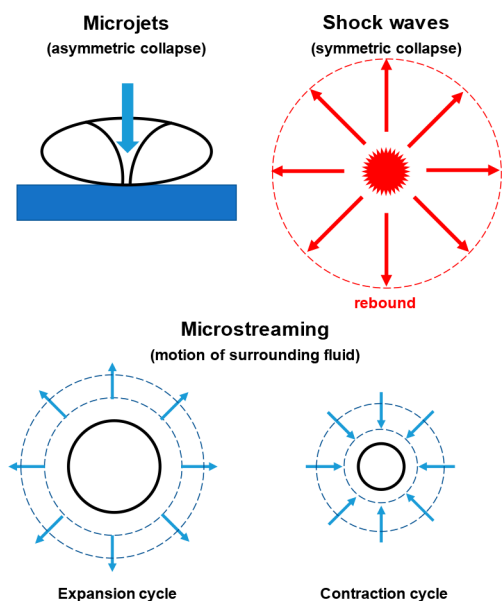


**Figure 1.** Illustration of the diversity of physical effects that may result due to acoustic perturbation (ultrasonic cavitation). Microjets arise from the asymmetrical collapse of cavitation bubbles due to the presence of a solid surface or another bubble. Shock waves are formed when a cavitation bubble collapses symmetrically. Microstreaming refers to the oscillating motion of the fluid in the vicinity of expanding and contracting bubbles. Finally, acoustic streaming (not shown) results in fluid flow due to acoustic (ultrasonic) propagation.

can be used to stimulate surface reactions. For example, on the basis of these concepts, ultrasonication has been used to promote the dissolution of minerals such as serpentine in applications related to  $\text{CO}_2$  mineralization.<sup>15</sup>

Despite a wide variety of applications, the mechanisms by which acoustic perturbation affects processes such as dissolution are not fully understood.<sup>16</sup> While high-speed photography and microscopy, and sonoluminescent characterization, have been used to study the interactions between cavitation bubbles and solid surfaces,<sup>8,17–19</sup> the role of the solute's composition and properties on the extent of dissolution stimulation remains less understood. To address this knowledge gap, this study investigates the dissolution kinetics of a wide range of minerals, whose dissolution rates vary by several orders of magnitude, both under sonicated and unsonicated conditions in aqueous solutions. For the first time, it is revealed from an energy landscape perspective how acoustic perturbation enhances mineral dissolution across a range of compositionally distinct minerals of widely differing hardnesses. Special focus is paid to reveal the mechanisms of acoustic perturbation on enhancing mineral dissolution.

## 2. METHODS

**2.1. Materials.** Phase-pure minerals including halite ( $\text{NaCl}$ ), gypsum ( $\text{CaSO}_4 \cdot 2\text{H}_2\text{O}$ ), calcite ( $\text{CaCO}_3$ ), serpentine (var antigorite:  $(\text{Mg,Fe})_3\text{Si}_2\text{O}_5(\text{OH})_4$ ), fluorite ( $\text{CaF}_2$ ), dolomite ( $\text{CaMg}(\text{CO}_3)_2$ ), orthoclase ( $\text{KAlSi}_3\text{O}_8$ ), and  $\alpha$ -quartz ( $\text{SiO}_2$ ) were sourced from Ward's Science.<sup>20</sup> A sodium aluminoborosilicate glass (NABS:  $0.83\text{SiO}_2 \cdot 0.11\text{B}_2\text{O}_3 \cdot 0.04\text{Na}_2\text{O} \cdot 0.01\text{Al}_2\text{O}_3$ ) and obsidian ( $0.81\text{SiO}_2 \cdot 0.09\text{Al}_2\text{O}_3 \cdot 0.05\text{K}_2\text{O} \cdot 0.05\text{Na}_2\text{O}$ ) were sourced from Vitro Minerals. For the batch dissolution experiments, the minerals were ground using an agate mortar and pestle and sieved to a particle size

ranging between 300 and 600  $\mu\text{m}$ . The size distribution of the particulates was measured using laser diffraction spectroscopy by dispersing the particulates in isopropanol at a wavelength of 750 nm. The surface area of the particulates was estimated by assuming a spherical geometry and on the basis of knowledge of their density. For dissolution experiments using vertical scanning interferometry (VSI, NewView 8200, Zygo Corporation), planar mineral surfaces of dimensions  $1.4 \text{ cm} \times 1.4 \text{ cm} \times 0.4 \text{ cm}$  ( $l \times w \times h$ ) were prepared by sectioning using a low-speed saw, and then polished with sandpaper (600 and 4000 grit, LECO Co.) using a lapping wheel (Ecomet 250, Buehler). For single-crystal calcite, nearly atomically smooth surfaces were prepared by cleaving using a razor blade. The presence of a solid surface larger than the bubble size ( $\approx 150 \mu\text{m}$ ) will cause asymmetric bubble collapse and the formation of microjets.<sup>11,12</sup> As such, acoustic perturbation as applied herein will produce microjets for both the planar and particulate solute systems. For a bubble far away from a rigid surface (i.e.,  $\gg r_{\text{max}}$ ), symmetric bubble collapse will result in the propagation of a spherical shock wave.<sup>19</sup>

In general, all samples were rinsed with Milli-Q (deionized, DI) water to remove fine particles. In addition, *tert*-butyl alcohol (TBA; ACS grade, >99%, Alfa Aesar) was used as a radical scavenger during sonication. It should be noted that this selection of minerals was made for the following reasons: (1) they are common to the earth's crust and feature relatively low solubilities (i.e., except for halite and gypsum), (2) they are slightly, if at all, affected by radicals due to the saturation of their valence state,<sup>21</sup> and (3) the wide range of hardnesses (over 1 order of magnitude) enables robust analysis of the solute's surface bond strength on dissolution under acoustic perturbation. Specifically, gypsum, calcite, fluorite, orthoclase, and quartz have hardnesses of 2, 3, 4, 6, and 7 on the Mohs scale thereby covering nearly the entire range of hardness observed in nature.

**2.2. Experimental Methods.** For particulate solids, in a batch reactor (Figure 2a), a horn type ultrasonic system (Fisher Scientific 550 Sonic Dismembrator; 500 W; 1.2  $\text{cm}^2$  tip area) was used to stimulate mineral dissolution. The reactor containing 50 mL of deionized (DI) water ( $\text{pH} = 5.8$ ) was maintained at isothermal conditions,  $25 \pm 0.5 \text{ }^\circ\text{C}$ , by circulating cooling water through a jacket that encased the sonoreactor. A range of solid-to-liquid ratios ( $s/l$ , units of  $\text{g/L}$ ) were considered wherein  $0.5 \text{ g/L} \leq s/l \leq 2.0 \text{ g/L}$  and used to match the surface area of the solute present under conditions of particle and planar sample dissolution. Ultrasonic waves were transmitted through the horn, under immersion, at 20 kHz (i.e., corresponding to a bubble size on the order of 150  $\mu\text{m}$ <sup>11</sup>) and a power of 250 W over the course of the experiments which encompassed a dissolution period of  $\approx 150$  min. The solution pH was measured using a calibrated ThermoScientific Ross Ultra electrode fitted with a temperature probe. The dissolution rates measured correspond to quantifications carried out under conditions of evolving (i.e., increasing), yet far from saturation conditions, of the solvent with respect to the dissolving solute.

TBA reacts rapidly with hydroxyl radicals (second-order rate constant,  $k = 6.0 \times 10^8 \text{ M}^{-1} \text{ s}^{-1}$ )<sup>22</sup> that form during ultrasonic cavitation, and therefore, it is often used as a radical scavenger. Such scavenging allows differentiation of the physical and chemical effects of sonication, so long as the addition of TBA does not markedly affect dissolution rates. As such, the prevalence of unique chemical effects (i.e., radical formation)

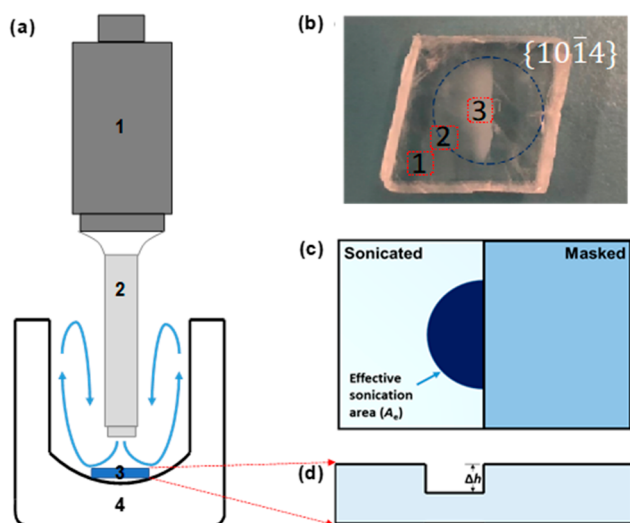


**Figure 2.** (a) Illustration of the experimental setup (1, transducer; 2, ultrasonic horn; 3, planar sample; and 4, water jacketed reactor), and (b) sonicated planar calcite sample (dimensions of  $1.4 \text{ cm} \times 1.4 \text{ cm} \times 0.4 \text{ cm}$ ,  $l \times w \times h$ ) showing surface alteration along the (c) top and (d) side views. It should be noted that particulate solutes were also used in addition to planar solute geometries. Here,  $A_e$  is the effective area ( $\text{m}^2$ ) that is exposed to sonication, and  $\Delta h$  (m) is the average height reduction that is induced due to solute dissolution.

of sonication can be assessed by comparing the dissolution rates of minerals in the presence and absence of TBA. In addition to sonicated conditions, control experiments were carried out under conditions of convective (mechanical) mixing to compare dissolution rates under convective conditions to those under conditions of sonication. Herein, the particle suspension was stirred at different mixing speeds between 350 and 1100 rpm using a magnetic stirrer (i.e., at different Reynolds numbers) to match or exceed the conditions of fluid flow as relevant under sonication action. [In a mechanically mixed system, the Reynolds number is defined as<sup>23</sup>  $Re_c = nL^2/\nu$ , where  $n$  is the mixing speed (rpm),  $L$  is the diameter of the agitator (m), and  $\nu$  is the kinematic viscosity of water ( $\text{m}^2/\text{s}$ ). In an acoustically stimulated system,  $Re_c$  is defined as<sup>24</sup>  $Re_c = v_c L_h/\nu$ , where  $v_c$  is the average circulation velocity (m/s), and  $L_h$  is the diameter of horn tip (m). Here, pressure ( $P_a$ ) propagation and fluid velocity ( $v$ ) follow an exponential decay:<sup>7</sup>  $P_a = P_{a,0} \exp(-\alpha s)$  and  $v = v_0 \exp(-\alpha s/2)$ , where  $P_{a,0}$  is the acoustic pressure at the horn tip,  $v_0$  is the initial fluid velocity due to sonication,  $\alpha$  is the attenuation coefficient, and  $s$  is the propagation distance. Following Wei et al. (2017),<sup>2</sup>  $P_{a,0}$ ,  $v_0$ , and  $\alpha$  for a 20 kHz system were estimated as 0.65 MPa,  $0.34 \text{ m s}^{-1}$ , and 0.10, respectively. Therefore, for a pressure propagation distance  $s = 2.07 \text{ cm}$ , the average circulation velocity was calculated as  $0.28 \text{ m/s}$ . This yields  $n = 330 \text{ rpm}$  which yields  $Re_c = 3900$ , indicating that fluid flow in the reactor is not in the turbulent region. Thus, achieving the same Reynolds number as that under conditions of sonication simply requires matching the rotational velocity of the stirrer ( $n$ ).]

For planar solids (Figure 2b), the mineral sample was fixed at the bottom of the jacketed reactor using a compliant silicone adhesive (Silicone Solutions SS-380). The sides and the top-half of the mineral surface were thereafter masked using the silicone adhesive to prevent the reaction of these surfaces with water, and to isolate them from acoustic perturbation. The

masked surface offers a height reference such that comparison of height changes of the reacted (unmasked surface) vis-à-vis the unreacted surface allows direct quantification of the mass loss and hence dissolution rate following sonication (Figure 2c,d). Sonication was applied immediately (i.e., within 1–2 s) after the solid and solution made contact. Following sonication, the silicone mask on the planar samples was peeled to expose the unreacted area. Thereafter, the surface topography was mapped using a vertical scanning interferometer (VSI; NewView 8200, Zygo Corporation) fitted with a  $100\times$  Mirau objective (numerical aperture, N.A. = 0.85) over a field-of-view (FOV) of  $87 \mu\text{m} \times 87 \mu\text{m}$  at a lateral resolution of 90 nm and at a vertical resolution of  $\pm 2 \text{ nm}$ . The surface topography images acquired were processed using Gwyddion (ver. 2.49)<sup>25</sup> to determine the change in surface area (roughness) and morphology following sonication.

**2.3. Analysis of Solution Compositions and Dissolution Rates.** Over the course of the particulate solute dissolution measurements, periodically, liquid volumes on the order of 0.5 mL were extracted at designated time intervals and subsequently filtered through  $0.1 \mu\text{m}$  filters for solution analysis. These samples were first diluted in a 5% concentrated (70%)  $\text{HNO}_3$  matrix prior to analysis. Thereafter, the concentrations of ions including Ca, Mg, Si, etc. were measured using inductively coupled plasma optical emission spectrometry (ICP-OES; PerkinElmer Avio 200). In general, over the period of measurement ( $\leq 2.5 \text{ h}$ ), the measured ion concentrations in solution showed a linear increase as a function of time for saturation determining species (e.g., Ca for the case of calcite). Therefore, the dissolution rate in the case of sonicated and sonication-free (convectively mixed) systems was simply compared by taking the ratio of the slopes of the concentration–time curves which yields the dissolution enhancement ratio ( $D_e$ , unitless). As such,  $D_e > 1$  implies a condition wherein sonication affects dissolution rates by more than just improving the mixing state of the solution. The actual dissolution rate of any mineral “ $i$ ” is written as  $D_i = m_i/S_{ai}$  where  $m_i$  is the slope of the concentration–time curve which remained linear (i.e., an indication of far-from-saturation mineral dissolution, mol/s), and  $S_{ai}$  is the total surface area of the solute ( $\text{m}^2$ ) for a given dilution ratio (herein,  $s/l = 2.0 \text{ g/L}$ ).

**2.4. Mineral Hardness.** The mineral’s hardness in terms of its Vickers Pyramid Number ( $H_v$ ) was measured using a microhardness tester (LM800AT, LECO Co.). Herein, following ASTM E384,<sup>26</sup> the mineral’s surface was indented by a pyramidal indenter with face angles of  $136^\circ$  with an applied load of 0.25–19.6 N depending on the hardness of the mineral to a penetration depth ( $d_p$ ) of  $19.2 \pm 4.8 \mu\text{m}$ . The mean diagonal length ( $d$ , mm) of the indentation was used to determine the hardness ( $H_v$ , GPa):<sup>26,27</sup>  $H_v = 0.0018544P/d^2$ , where  $P$  is the force (N) and  $A_s$  is the surface area of the indentation ( $\text{mm}^2$ ).

### 3. RESULTS AND DISCUSSION

Acoustic perturbation in a sonoreactor (Figure 2a) is postulated to enhance dissolution by improving mass transfer in solution (i.e., by mixing), and at the solid–liquid interface,<sup>28</sup> and/or by increasing the reactive surface area of the solute through interparticle collision, particle-shockwave/microjet interaction, particle-horn collision, and particle-(reactor) wall collision,<sup>29</sup> e.g., due to mechanical abrasion and/or fracture (comminution).

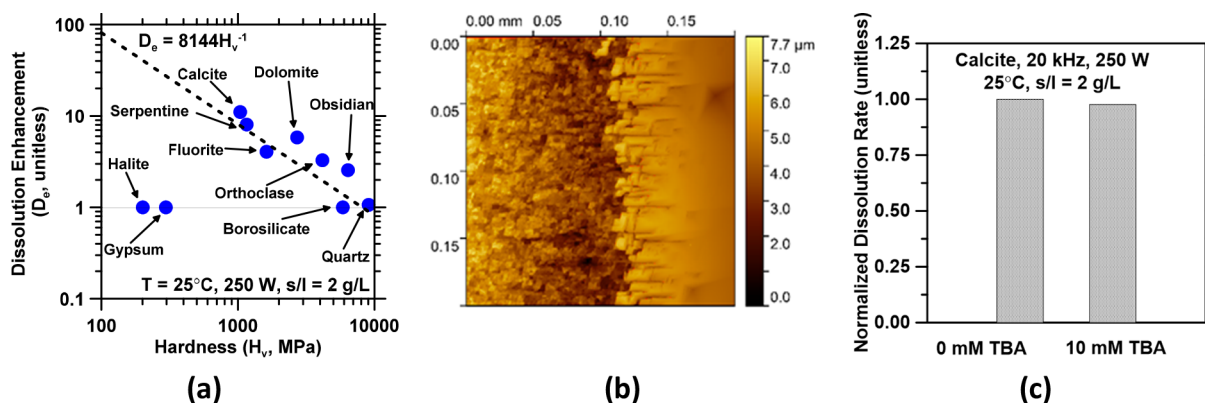


**Figure 3.** (a) Dissolution enhancement produced under the action of acoustic perturbation as a function of the mineral's hardness, a readily measurable property. [As a point of reference, the dissolution rates of calcite, obsidian, and orthoclase as shown in Figure 3a under sonication-free conditions (i.e., under conditions of convective mixing) were measured as being  $4.86 \times 10^{-7}$  mol/m<sup>2</sup>/s,  $1.63 \times 10^{-11}$  mol/m<sup>2</sup>/s, and  $2.42 \times 10^{-9}$  mol/m<sup>2</sup>/s, at 25 °C and 1 bar, respectively.] The data is fitted by a power-law expression of the form  $D_e = AH_v^B$ , where  $A$  (8144, MPa) and  $B$  (−1) are fitting coefficients. On account of their very soft nature, and fast dissolution rates, halite and gypsum do not follow the dissolution scaling. (b) The roughening produced on a planar calcite surface following acoustic perturbation. The masked (smooth) surface is prevented from dissolving by applying a highly compliant silicone coating to it. Following sonication (and dissolution), for the planar surface, roughening results in a surface area that is 3.5× larger than the surface area of the pristine (unsonicated and undissolved) calcite surface. (c) The dissolution rate of calcite measured under acoustic perturbation in the presence (10 mM) of or in the absence (0 mM) of the radical scavenger *tert*-butyl alcohol (TBA).

Continuing on, Figure 3a shows that the dissolution enhancement ( $D_e$ , unitless ratio, i.e., the ratio of the dissolution rate under acoustic perturbation to the dissolution rate measured under conditions of mechanical mixing) produced by acoustic perturbation, i.e., vis-à-vis the scenario of convective mixing, increases with decreasing mineral hardness. Interestingly, it is noted that the dissolution enhancement scales as a function of  $x^{-1}$ , where  $x$  is the mineral's hardness ( $H_v$ , MPa). It is noted that the inverse scaling of dissolution enhancement as a function of mineral hardness does not capture the behavior of halite and gypsum, i.e., rather soft and fast dissolving minerals that experience no dissolution enhancement under sonication ( $D_e \approx 1$ ). Furthermore, it appears as though no dissolution enhancement would be produced for minerals with a hardness larger than 8000 MPa. This suggests a domain, i.e., characterized by hardness and dissolution rates, over which dissolution enhancement can be most effectively exploited, below and above which acoustic perturbation may not be an effective means of altering dissolution rates. It is worth noting that both dissolution kinetics and hardness have been reported to be controlled by the topology of the atomic network; namely, dissolution kinetics and hardness decrease and increase with increasing network connectivity, respectively.<sup>30,31</sup> The results presented in Figure 3a further support this previously elucidated relationship between dissolution kinetics and hardness.

Further, Figure 3a highlights that the dissolution enhancement produced is a function of the solute's resistance to mechanical deformation, i.e., since hardness is an indicator of resistance to elastoplastic deformations.<sup>32</sup> Importantly, this holds true not only for crystalline solids, i.e., which feature an orientational dependence, but also for isotropic (i.e., disordered) solids such as obsidian and a synthetic borosilicate glass composition. The substantial decrease in dissolution enhancement with increasing hardness, e.g., for quartz where the dissolution rate elevates by only 1.06× (as opposed to calcite, 11.1×), may suggest that acoustic perturbation simply elevates the surface area available for dissolution,  $S_a$ , i.e., since the increase in surface area induced will also inversely scale

with hardness. Rather, as will be discussed below, the mechanism of acoustically stimulated dissolution is more complex and cannot be explained by the increase in surface area that is far smaller than the extent of dissolution enhancement. For example, surface topography analysis of planar, sonicated calcite surfaces (e.g., see Figure 3b wherein a surface area increase of  $\approx 3.5\times$  results) show substantial surface roughening and exposure, following acoustic perturbation. {The particle velocity imparted under the action of shock waves can be estimated as<sup>10</sup>  $v = (Pr/6\mu)[1 - \exp(-9\mu\Delta t/2\rho r^2)]$ , where  $P$  is the pressure (Pa) of shockwaves,  $r$  is the particle radius (m),  $\rho$  is the particle density (kg/m<sup>3</sup>),  $\mu$  is the fluid viscosity (Pa s), and  $\Delta t = 10^{-8}/r$ . This analysis reveals that the velocities of particle collision are relatively small,  $\leq 5.2$  m/s at a distance of one  $r_{\text{max}}$  (maximum bubble size), indicating that particle–particle collisions are not expected to be a substantial contributor to fracture, and surface area creation.} Similarly, analysis of surface areas pre- and postsonication for calcite particulates highlights a surface area increase of around 1.94×, i.e., from analysis of light scattering data. However, our analysis reveals a substantial mismatch between the observed increase in dissolution rates ( $\approx 11.1\times$  for calcite particulates) and the associated surface area enhancement ( $\approx 1.94\times$  for calcite particulates). In other words, at most 18% of the dissolution enhancement is attributable to an increase in surface area. Moreover, as seen in Figure 3c, the formation of radicals during sonication does not measurably alter dissolution rates. This data highlights that the typical explanations attributable to sonication, i.e., surface area amplification, and radical formation, do not fully explain the dissolution enhancement that is produced by sonication.

To more closely examine the physical effects of cavitation on dissolution enhancement calcite was analyzed as an exemplar solute because it is (a) the softest solute which shows a dissolution enhancement, and (b) the sample that is most susceptible to surface area amplification. First, the morphology of planar calcite surfaces was characterized using vertical scanning interferometry and scanning electron microscopy. As shown in Figure 4a (i.e., area 1 shown in Figure 2b), outside

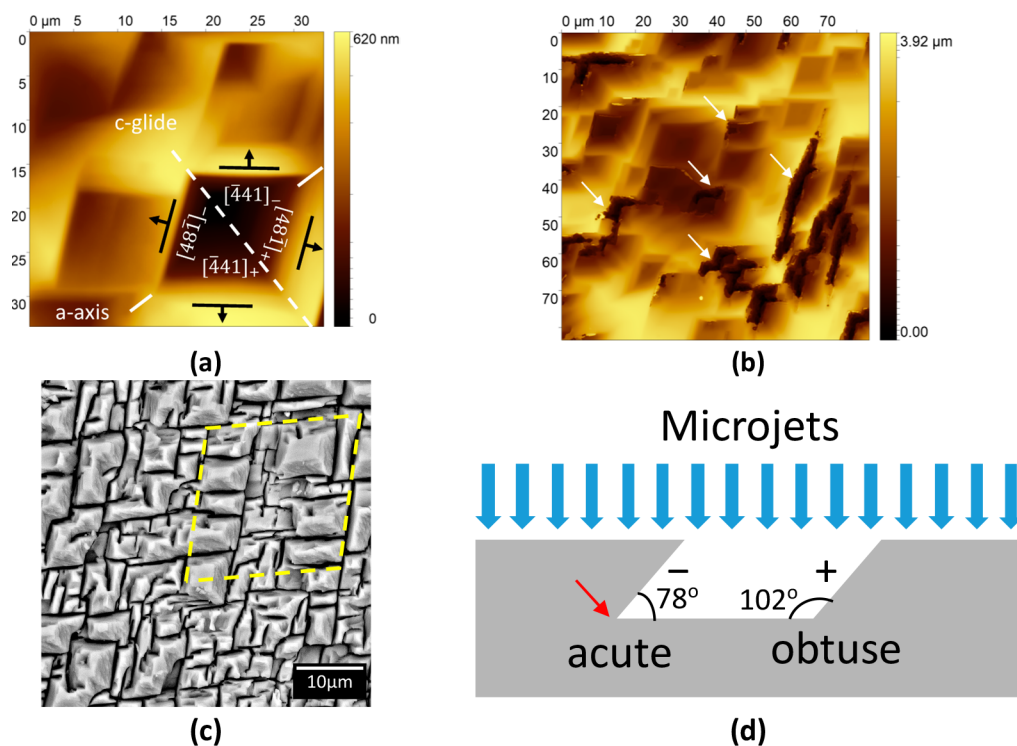


**Figure 4.** Surface morphology and topographical maps of  $\{10\bar{1}4\}$  calcite surfaces: (a) where only etch pits can be observed (i.e., outside of the effective sonication zone), (b) at the sonication boundary where microcleavages emerge at the  $[\bar{4}41]_-$  and  $[48\bar{1}]_-$  steps (marked by arrows), and (c) at the center of the sonication zone where bridging of the microcleavages occurred. The rhomboid drawn in yellow features internal angles of  $78^\circ$  and  $102^\circ$ . (d) An illustration of the geometry of the pits produced on calcite surfaces (e.g., as observed in part a).

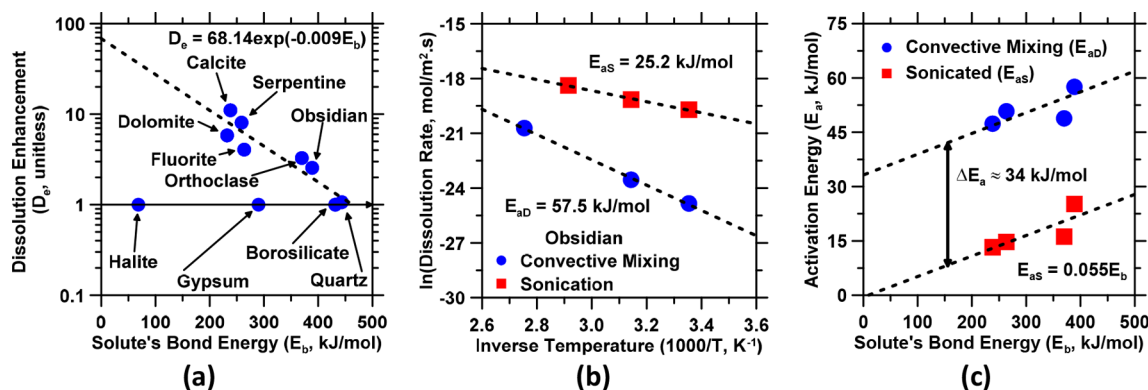


**Figure 5.** (a) Dissolution enhancement produced under the action of acoustic perturbation as a function of the solute's average bond energy. The data is fitted by an Arrhenius-like expression of the form  $D_e = C \exp((-f/RT)E_b)$  where  $D_e$  is the dissolution enhancement (unitless),  $C$  is a dissolution constant (68.14),  $f$  is a scaling factor ( $\approx 0.022$ , unitless),  $E_b$  is the bond energy (kJ/mol),  $R$  is the gas constant, and  $T$  is the temperature. In general, on account of their overly soft nature, and fast dissolution rates, halite and gypsum do not follow the dissolution scaling(s). (b) An Arrhenius plot showing the activation energy of dissolution of obsidian ( $E_{aD} = 57.5$  kJ/mol) under conditions of convective mixing, i.e., “unsonicated”, and under the action of sonication ( $E_{aD} = 25.2$  kJ/mol). Frequency factors are estimated by extrapolation of the linear fit to infinite temperature. (c) The activation energies of dissolution under unsonicated and sonicated conditions. For solutes including calcite, fluorite, orthoclase, and obsidian, a linear scaling of activation energy and solute bond strength is revealed wherein the average difference in activation energy between unsonicated and sonicated conditions remains constant,  $\Delta E_a = E_{aD} - E_{aS} \approx 34$  kJ/mol.

the sonication region rhombohedral etch pits form during the dissolution of  $\{10\bar{1}4\}$  unsonicated calcite surfaces which are defined by crystallographic steps normal to the  $[\bar{4}41]_-$  and  $[48\bar{1}]_-$  planes, respectively. The anisotropic arrangement of carbonate groups results in such patterns wherein the paralleled  $[\bar{4}41]_-$  and  $[48\bar{1}]_-$  steps form an acute angle ( $78^\circ$ ) with the  $\{10\bar{1}4\}$  cleavage plane while the  $[\bar{4}41]_+$  and  $[48\bar{1}]_+$  steps produce an obtuse angle ( $102^\circ$ ) with the  $\{10\bar{1}4\}$  plane (see Figure 4d).<sup>33,34</sup> On the other hand, at the boundary

of the sonicated and unsonicated zones (i.e., area 2 in Figure 2b and Figure 4b), microcleavages which parallel the  $[\bar{4}41]_-$  and  $[48\bar{1}]_-$  steps were observed as shown in Figures 3b and 4b,c. Finally, in the center of the sonication zone (i.e., area 3 in Figure 2b), the surface is covered by large cleavages that form by coalescence of the microcleavages generated along the  $[\bar{4}41]_-$  and  $[48\bar{1}]_-$  steps (see Figure 4c). Once again, these cleavage planes form a characteristic rhomboid structure that features internal angles of  $78^\circ$  and  $102^\circ$ . As such, upon

sonication, as the dissolution of calcite forms rhombohedral etch pits, stresses concentrate at the vertex of the acute (angled) steps. This results in the formation of microcleavages along the  $[4\ 41]_{-}$  and  $[48\bar{1}]_{-}$  steps resulting in *patterned* surface roughening. These observations align with those of Wagterveld et al. (2011) who reported that cavitation induces breakage of the crystal structure of calcite resulting in large planes of cleavage similar to those observed herein.<sup>18</sup> Such damage increases the surface area of calcite by 3.5× the initial surface area as noted above.

Coming back to the attributes of the mineral solute, for an ideal, defect-free, compositionally homogeneous solid, its hardness is known to scale with the bond energy (and the volume density of interatomic bonds).<sup>35</sup> For example, Gao et al. (2003) reported that the hardness of covalent solids increases with bond energy (ionicity)<sup>36</sup> whereas Šimůnek and Vackář (2006) highlighted that hardness is correlated to the bond energy.<sup>37</sup> Furthermore, Roberts et al. also showed that the hardness of organic solids is a linear function of the cohesive energy density.<sup>38–40</sup> These concepts are well-borne-out by the inverse scaling of dissolution enhancement with hardness as noted in Figure 3a. Therefore, we calculated the composite bond energies of the different solutes, i.e., using a mixture rule as a function of the solute's molar composition, and the strength of its interatomic bonds (e.g., a Ca–O bond which features a rupture energy of 133.9 kJ/mol). First, it is expectedly noted that hardness is correlated with the composite bond energy (not shown). Second, significantly, when we cast the extent of dissolution enhancement as a function of the composite bond energy (see Figure 5a), the trends in the data are fitted by an equation of the form  $D_e = C \exp((-f/RT)E_b)$  where  $D_e$  is the dissolution enhancement (unitless),  $C$  is a dissolution constant (68.14, unitless) that is related to the solution chemistry (i.e., herein, a solvent that features a circumneutral pH),  $f$  is a scaling factor (0.022, unitless),  $E_b$  is the composite bond energy (kJ/mol),  $R$  is the gas constant (8.314 J/mol K), and  $T$  is the temperature (298.15 K). Here, the product  $fE_b$  reveals the energy imparted to the solute under acoustic perturbation which ranges  $2.1k_B T \leq fE_b \leq 4.1k_B T$ , i.e., from the softest (calcite) to the hardest mineral (quartz), respectively, in order of ascending bond energy, where  $k_B$  is the Boltzmann constant. The fitting shown in Figure 5a reveals the energy imparted by acoustic perturbation, that enhances dissolution, across the entire range of solute compositions and structures (crystalline and disordered), although not for halite or gypsum, and vanishingly so for solids such as borosilicate glass, and quartz for which  $H_v > 8000$  MPa.

The substantial dissolution enhancement noted in Figure 5a, under macroscopically isothermal conditions (as confirmed by separate measurements of solution temperature within the sonoreactor), suggests that acoustic stimulation may decrease the activation energy of dissolution. Indeed, a comparison of the activation energies of dissolution under sonicated and unsonicated conditions, for calcite, fluorite, obsidian, and orthoclase (see Figure 5b,c), reveals that sonication significantly reduces the activation energy. Indeed, on average across a range of minerals it is shown that the energy imparted by sonication, i.e., on the order of a few  $k_B T$ , greatly reduces the activation energy of dissolution, although by a fixed amount across a range of solutes such that  $\Delta E_a = E_{aD} - E_{aS} \approx 34$  kJ/mol. This energy imparted (e.g., due to the action of shock waves, or microjets) is transported across the solute–solvent

interface. Furthermore, it is observed that (see Figure 5c) that the activation energy of dissolution, i.e., both under sonicated and sonication-free conditions, scales with averaged bond energy. However, this reduction in activation energy is not expected to be on account of the increase in the surface area, because while surface area can enhance dissolution rates, it does not influence the activation barrier of the process.<sup>41</sup> In addition, the change in the activation energy is not expected to be on account of sonication inducing a dramatic local increase in temperature at the solute–solvent interface (i.e., by affecting the reaction temperature term,  $T$ ) since the sonoreactor is robustly thermostated. As a result, local heating, even if it occurs, is expected to be rapidly dissipated into the cooling water circuit ensuring that macroscopically isothermal conditions are maintained. As such, it can be concluded that sonication in the manner applied herein (i.e., under relevant conditions of frequency, and power) imparts energy to the solute's surface atoms which eases their extraction into the solvent (i.e., dissolution): an effect that scales with the solute's bond energy. It should moreover be noted that, as noted in Figure 5c, for solutes with  $E_b \leq 365$  kJ/mol, under sonication,  $E_{aS} \leq 20$  kJ/mol. This should not however be considered as a switch of the dissolution mechanism, i.e., from interface to transport controlled dissolution, since as shown by Rimstidt and Barnes,<sup>42</sup> and Rimstidt and Dove,<sup>43</sup> the magnitude of the activation energy alone is not a reliable indicator of the dissolution mechanism, or changes therein. Note that, however, by analyzing the dissolution data within the Eyring formalism, we find that the activation enthalpy (and the change therein upon sonication) closely mimics the trends in the activation energy and is accordingly reduced in a similar fashion upon sonication (not shown). This confirms that the decrease in the activation energy is not attributable to an artifact of the Arrhenius analysis.

Coming back to the case of calcite, i.e., the softest mineral that should be most affected by surface area effects, the effects of sonication can be rationalized as follows. Under the effect of sonication, the surface area increase that results for calcite particulates is nominal, i.e., 1.94× for calcite particulates. On the other hand, the measured increase in the dissolution rate (i.e., dissolution enhancement) for calcite particulates is on the order of 11.1× (see also Section 2.3). Since dissolution rates are proportional to surface area (i.e., assuming reactive surface area scales with total surface area;<sup>44</sup> although this does not have to obey a 1:1 scaling), at best, the increase in surface area should produce an increase in dissolution rates, of calcite particulates, of 1.94×, i.e., a mismatch of nearly 5.7×. Second, while it is likely reasonable to conclude that cavitation may result in modest local heating<sup>45</sup> and hence kinetic acceleration of dissolution rates, based on the activation energy of calcite dissolution at circumneutral pH, i.e., around 35 kJ/mol, a sustained temperature on the order of 65 °C would be needed to induce a dissolution enhancement on the order of 11.1×, for calcite. Given that the sonoreactor is robustly thermostated and that the solution therein is well-mixed, any temperature rise, even if produced, is expected to be rapidly dissipated into the circulating coolant water.

Based on this reasoning, the effects of acoustic perturbation can be explained from an energy landscape perspective under macroscopically isothermal conditions as follows. Specifically, it is postulated that cavitation and the resultant transmission of shockwaves/microjets that contact the solute impart focused energy to the solute's surface. (This implies that a few  $k_B T$  of

focused energy applied to the solute's surface is a far more effective means of stimulating dissolution than increasing surface area.) This results in a perturbation (i.e., wherein the atomic displacement produced scales with the energy input, see Figure 5a) of surface atoms from their equilibrium positions. Consequently, under sonication, the system achieves a higher-energy metastable state that is closer to the transition state (see Figure 6). It should be noted that although our

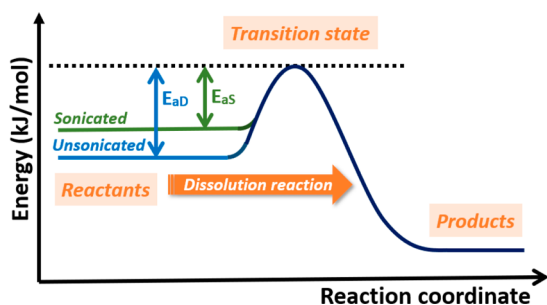


**Figure 6.** Schematic which shows how sonication eases the dissolution process as a result of which excited reactant solute atoms need a smaller amount of energy vis-à-vis unsonicated atoms to achieve their transition state resulting in mineral dissolution (not to scale).

analysis shows that the activation energy is decreasing (see Figure 5c), such a decrease may, in principle, result from (i) an increase in the energy of the solute (as postulated herein), or (ii) a decrease in the energy of the intermediate transition state. Although we are unable to irrefutably clarify which of these is dominant, the fact that the magnitude of the decrease in activation energy and attempt frequency is fairly constant over all the minerals evaluated suggests that sonication indeed destabilizes the mineral (i.e., rather than changing the nature of the intermediate transition state formed during dissolution). As a result, the “excited” atoms of the mineral solute then need only a small amount of energy for dissolution to proceed by the rupture of atomic bonds. It is important to note that the amount of energy imparted is subcritical, i.e., sufficient to motivate dissolution, but insufficient to directly induce bond rupture (i.e., fracture, which would manifest in the form of an increase in surface area proportionate to the level of dissolution enhancement, see also Figure 4). This subcritical energy imparted by sonication results in a lowering of the activation barrier of dissolution under sonicated conditions such that  $E_{aS} < E_{aD}$  (see Figure 5b,c). Herein, assuming that the metastable excited state remains locally harmonic, the decrease in the curvature of the local energy basin (see Figure 6) is associated with a concurrent decrease in the oscillation attempt frequency with increasing energy of the solute atoms (i.e., following Kramers’ formalism<sup>46,47</sup>), as espoused by the *compensation rule*<sup>48</sup> (note that, implicitly, this also suggests a difference in the Maxwell–Boltzmann distribution of the energies of solute atoms under sonicated as compared to unsonicated conditions). Indeed, this is expected, as the relationships shown in Figure 5a–c require that if the activation energy reduces by a fixed amount from unsonicated to sonicated conditions, this has to be accompanied by a correspondent reduction in the attempt frequency of a chemical reaction wherein the extent of reduction scales with the bond energy. It should be further noted that an inherent assumption in this reasoning is that the structure and free energy of the transition state remain

unchanged under both sonicated and unsonicated conditions. This assumption is made on the basis that the effects of sonication are ballistic; i.e., sonication imparts momentum to surficial atoms, but does not induce electronic effects. However, if sonication were to induce electronic effects, e.g., by altering chemical bonding in the solvent environment vis-à-vis the solute, e.g., at the solute–solvent interface and thereby stabilizing alternate transition states, it is indeed conceivable that the effects of sonication create an alternate (low-energy) pathway along the potential energy hypersurface (e.g., by accessing otherwise forbidden states) as a result of which dissolution is eased and facilitated. If so, these effects would be similar to those observed in heterogeneous catalytic reactions wherein microporous solids and/or cosolvents increase the rates of chemical reaction by inducing a lower activation barrier pathway via selective solvation of transition states relative to the reactants.<sup>49,50</sup> In any event, it is suggested that it is shockwave/microjet-imparted energy (momentum) transfer that produces a reduction in the activation energy that is the primary mechanism by which acoustic perturbation results in elevating mineral (solute) dissolution rates under macroscopically isothermal conditions.

#### 4. CONCLUSIONS

Acoustic perturbation, e.g., ultrasonication, offers a means to control and expedite a range of interfacial reaction processes including dissolution, precipitation, and particle agglomeration. Herein, acoustic perturbation is demonstrated as a means for isothermal stimulation of mineral dissolution processes across a range of mineral compositions with widely differing hardnesses and bond energies. Specifically, it is shown that the dissolution enhancement ( $D_e$ ) induced under acoustic perturbation ranges between 11.1× for calcite (Mohs hardness: 3) and 1.06× for quartz (Mohs hardness: 7). It is shown that the extent of dissolution enhancement is described by an Arrhenius-like expression of the form  $D_e = C \exp((-f/RT)E_b)$ , where the product  $fE_b$  reveals the energy imparted by acoustic stimulation to atoms on the solute’s surface. The analysis indicates that sonication in the manner applied herein reduces the energy barrier to mineral dissolution by a fixed amount such that  $\Delta E_a = E_{aD} - E_{aS} \approx 34$  kJ/mol, an outcome that is supported by separate measurements of the activation energies of a variety of solutes under sonication action. From an energy landscape perspective, it is proposed that sonication results in the perturbation of the solute’s surface atoms from their equilibrium positions. As a result, upon contact with a solvent, such excited atoms need only an incremental amount of energy to achieve their transition state and for dissolution to occur by the rupture of atomic bonds on the solute’s surface. Therefore, the activation energy of dissolution under sonication is substantially smaller than that under sonication-free conditions. It is this nature of atomic excitation that explains how acoustic perturbation enhances mineral dissolution processes under macroscopically isothermal conditions.

On the basis of observations on a wide range of mineral solutes it is noted that acoustic perturbation offers a means for unparalleled stimulation of mineral dissolution processes. However, there appear to be limits to the success of this approach. For example, acoustic perturbation is broadly unable to excite the dissolution of halite and gypsum, soft, rapidly dissolving minerals. This suggests a lower bound and upper bound of mineral hardness (and bond energy), below and above which dissolution cannot be appreciably stimulated.

Nevertheless, the extent of stimulation produced is significant for the following reasons: (a) it does not require the use of stoichiometric chemical additives that cannot be reused or recovered (easily), (b) broadly speaking, the extent of enhancement is more substantial than that typically achievable using stoichiometric additives, and (c) it can be accomplished at macroscopically isothermal conditions. Furthermore, while the present approach has only considered monochromated sonication (i.e., at 20 kHz, 250 W), it is indeed expected that acoustic perturbation, if applied at the resonance frequency of the solute, may be an energetically even more efficient, and further improved, means of dissolution stimulation, e.g., by inducing harmonic amplification of atomic perturbation and surface area creation by causing solute fracture in addition to atomic perturbation. From a more practical perspective, the extent of dissolution enhancement produced offers a means to mobilize reactant species in solution at near ambient and isothermal conditions across a diversity of reactants. While unarguably this requires the expenditure of energy (e.g., electricity from renewable sources) for acoustic perturbation, it offers a means to bypass thermal activation and/or intensive grinding, i.e., the typical and potentially far more energy intensive pathways that are followed to ensure the rapid mobilization of ionic species in aqueous dissolution from mineral reactants. For example, acoustic stimulation of the nature proposed herein could be applied to create new routes for the low-temperature synthesis of cementation agents from geological precursors (rocks), new routes for chemical–mechanical polishing, and routes for creating alternatives to mechanical grinding as a pathway for particle comminution and reactivity enhancement.

## AUTHOR INFORMATION

### Corresponding Author

\*Phone: (310) 206-3084. E-mail: [gsant@ucla.edu](mailto:gsant@ucla.edu).

### ORCID

Zongsu Wei: 0000-0001-8747-2251

Yi-Hsuan Hsiao: 0000-0002-0359-5439

Erika Callagon La Plante: 0000-0002-5273-9523

Dante Simonetti: 0000-0002-5708-460X

Laurent Pilon: 0000-0001-9459-8207

Mathieu Bauchy: 0000-0003-4600-0631

Jacob Israelachvili: 0000-0001-8915-8741

Gaurav Sant: 0000-0002-1124-5498

### Author Contributions

<sup>†</sup>Z.W. and Y.-H.H. contributed equally to this work.

### Notes

The authors declare no competing financial interest.

## ACKNOWLEDGMENTS

The authors acknowledge financial support for this research from the Department of Energy, Office of Fossil Energy via the National Energy Technology Laboratory (NETL: DE-FE0029825), The Anthony and Jeanne Pritzker Family Foundation, Department of Energy's Nuclear Energy University Program (DOE-NEUP: DE-NE0008398), and the National Science Foundation (CAREER Award: 1253269, CMMI: 1562066). This research was conducted in the Laboratory for the Chemistry of Construction Materials (LC<sup>2</sup>) at UCLA. As such, the authors gratefully acknowledge the support that has made these laboratories and their

operations possible. The contents of this paper reflect the views and opinions of the authors, who are responsible for the accuracy of the datasets presented herein, and do not reflect the views and/or policies of the funding agencies, nor do the contents constitute a specification, standard, or regulation. The authors also acknowledge Dr. Joseph King (ARPA-E, U.S. Department of Energy) for numerous stimulating discussions of dissolution amplification by acoustic perturbation.

## REFERENCES

- (1) Suslick, K. S. Sonochemistry. *Science* **1990**, *247*, 1439–1445.
- (2) Wei, Z.; Villamena, F. A.; Weavers, L. K. Kinetics And Mechanism Of Ultrasonic Activation Of Persulfate: An In Situ EPR Spin Trapping Study. *Environ. Sci. Technol.* **2017**, *51*, 3410–3417.
- (3) Didenko, Y. T.; McNamara, W. B.; Suslick, K. S. Hot Spot Conditions During Cavitation In Water. *J. Am. Chem. Soc.* **1999**, *121*, 5817–5818.
- (4) Mason, T. J.; Lorimer, J. P. *Sonochemistry—Theory, Applications And Uses Of Ultrasound In Chemistry*; Wiley-Interscience Publication: New York, 1988.
- (5) Mason, T. J.; Lorimer, J. P. *Applied Sonochemistry: The Use Of Power Ultrasound In Chemistry And Processing*; Wiley-VCH Verlag GmbH: Weinheim, 2002.
- (6) Sillanpää, M.; Pham, T.-D.; Shrestha, R. A. In *Ultrasound Technology In Green Chemistry*; Springer Netherlands: Dordrecht, 2011; pp 1–21.
- (7) Leighton, T. G. *The Acoustic Bubble*; Academic Press: San Diego, CA, 1994.
- (8) Ohl, S. W.; Klaseboer, E.; Khoo, B. C. Bubbles With Shock Waves And Ultrasound: A Review. *Interface Focus* **2015**, *5*, 20150019.
- (9) Lamminen, M. Mechanisms And Factors Influencing The Ultrasonic Cleaning Of Particle-Fouled Ceramic Membranes. *J. Membr. Sci.* **2004**, *237*, 213–223.
- (10) Prozorov, T.; Prozorov, R.; Suslick, K. S. High Velocity Interparticle Collisions Driven By Ultrasound. *J. Am. Chem. Soc.* **2004**, *126*, 13890–13891.
- (11) Doktycz, S. J.; Suslick, K. S. Interparticle Collisions Driven By Ultrasound. *Science* **1990**, *247*, 1067–1069.
- (12) Suslick, K. S. *Ultrasound: Its Chemical, Physical, And Biological Effects*; VCH Publishers: New York, 1988.
- (13) Thompson, L. H.; Doraiswamy, L. K. The Rate Enhancing Effect Of Ultrasound By Inducing Supersaturation In A Solid-Liquid System. *Chem. Eng. Sci.* **2000**, *55*, 3085–3090.
- (14) Suslick, K.; Casadonte, D.; Doktycz, S. The Effects Of Ultrasound On Nickel And Copper Powders. *Solid State Ionics* **1989**, *32–33*, 444–452.
- (15) Park, A. H. A.; Fan, L. S. CO<sub>2</sub> Mineral Sequestration: Physically Activated Dissolution Of Serpentine And PH Swing Process. *Chem. Eng. Sci.* **2004**, *59*, 5241–5247.
- (16) Shchukin, D. G.; Skorb, E.; Belova, V.; Möhwald, H. Ultrasonic Cavitation At Solid Surfaces. *Adv. Mater.* **2011**, *23*, 1922–1934.
- (17) Holzfuss, J.; Rüggeberg, M.; Billo, A. Shock Wave Emissions Of A Sonoluminescing Bubble. *Phys. Rev. Lett.* **1998**, *81*, 5434–5437.
- (18) Wagterveld, R. M.; Boels, L.; Mayer, M. J.; Witkamp, G. J. Visualization Of Acoustic Cavitation Effects On Suspended Calcite Crystals. *Ultrason. Sonochem.* **2011**, *18*, 216–225.
- (19) Ohl, C. D.; Kurz, T.; Geisler, R.; et al. Bubble Dynamics, Shock Waves And Sonoluminescence. *Philos. Trans. R. Soc., A* **1999**, *357*, 269–294.
- (20) Lenhart, J. J.; Saiers, J. E. Transport Of Silica Colloids Through Unsaturated Porous Media: Experimental Results And Model Comparisons. *Environ. Sci. Technol.* **2002**, *36*, 769–777.
- (21) Whitten, K. W.; Davis, R. E.; Peck, M. L.; Peck, M. L. *General Chemistry*, 6th ed.; Cengage Learning: Boston, MA, 2000.
- (22) Buxton, G. V.; Greenstock, C. L.; Helman, W. P.; Ross, A. B. Critical Review Of Rate Constants For Reactions Of Hydrated Electrons, Hydrogen Atoms And Hydroxyl Radicals ( $\cdot\text{OH}/\cdot\text{O}^-$  In Aqueous Solution). *J. Phys. Chem. Ref. Data* **1988**, *17*, 513–886.

- (23) Kramers, H.; Baars, G. M.; Knoll, W. H. A Comparative Study On The Rate Of Mixing In Stirred Tanks. *Chem. Eng. Sci.* **1953**, *2*, 35–42.
- (24) Vichare, N. P.; Gogate, P. R.; Dindore, V. Y.; Pandit, A. B. Mixing Time Analysis Of A Sonochemical Reactor. *Ultrason. Sonochem.* **2001**, *8*, 23–33.
- (25) Nečas, D.; Klapetek, P.; Anderson, C.; Šiler, M.; Bílek, J.; Ocelic, N.; Zitko, R.; Chvátal, L.; Neumann, S.; Hořák, J. *Gwyddion*; Czech Metrology Institute, 2017.
- (26) ASTM. *Standard Test Method For Knoop And Vickers Hardness Of Materials (E384-11)*. ASTM International 2011.
- (27) Yamane, M.; Mackenzie, J. Vicker's Hardness Of Glass. *J. Non-Cryst. Solids* **1974**, *15*, 153–164.
- (28) Adewuyi, Y. G. Sonochemistry: Environmental Science And Engineering Applications. *Ind. Eng. Chem. Res.* **2001**, *40*, 4681–4715.
- (29) Zeiger, B. W.; Suslick, K. S. Sonofragmentation Of Molecular Crystals. *J. Am. Chem. Soc.* **2011**, *133*, 14530–14533.
- (30) Pignatelli, I.; Kumar, A.; Bauchy, M.; Sant, G. Topological Control On Silicates' Dissolution Kinetics. *Langmuir* **2016**, *32*, 4434–4439.
- (31) Smedskjaer, M. M.; Mauro, J. C.; Yue, Y. Prediction Of Glass Hardness Using Temperature-Dependent Constraint Theory. *Phys. Rev. Lett.* **2010**, *105*, 115503.
- (32) Bhattacharya, A. K.; Petrovic, J. J. Hardness And Fracture Toughness Of Sic-Particle-Reinforced Mosi<sub>2</sub> Composites. *J. Am. Ceram. Soc.* **1991**, *74*, 2700–2703.
- (33) Liang, Y.; Baer, D. R. Anisotropic Dissolution At The Caco<sub>3</sub>(10 $\bar{1}$ 4)—Water Interface. *Surf. Sci.* **1997**, *373*, 275–287.
- (34) Hillner, P. E.; Gratz, A. J.; Manne, S.; Hansma, P. K. Atomic-Scale Imaging Of Calcite Growth And Dissolution In Real Time. *Geology* **1992**, *20*, 359.
- (35) Zheng, Q.; Yue, Y.; Mauro, J. C. Density Of Topological Constraints As A Metric For Predicting Glass Hardness. *Appl. Phys. Lett.* **2017**, *111*, 011907.
- (36) Gao, F.; He, J.; Wu, E.; Liu, S.; Yu, D.; Li, D.; Zhang, S.; Tian, Y. Hardness Of Covalent Crystals. *Phys. Rev. Lett.* **2003**, *91*, 015502.
- (37) Šimůnek, A.; Vackář, J. Hardness Of Covalent And Ionic Crystals: First-Principle Calculations. *Phys. Rev. Lett.* **2006**, *96*, 085501.
- (38) Roberts, R. J.; Rowe, R. C.; York, P. The Relationship Between Indentation Hardness Of Organic Solids And Their Molecular Structure. *J. Mater. Sci.* **1994**, *29*, 2289–2296.
- (39) Sher, A.; Chen, A.-B.; Spicer, W. E. Dislocation Energies And Hardness Of Semiconductors. *Appl. Phys. Lett.* **1985**, *46*, 54–56.
- (40) Tian, Y.; Xu, B.; Zhao, Z. Microscopic Theory Of Hardness And Design Of Novel Superhard Crystals. *Int. J. Refract. Hard Met.* **2012**, *33*, 93–106.
- (41) Boudart, M.; Djéga-Mariadassou, G. *Kinetics Of Heterogeneous Catalytic Reactions*; Princeton Univ Press, 2014.
- (42) Rimstidt, J. D.; Barnes, H. L. The Kinetics Of Silica-Water Reactions. *Geochim. Cosmochim. Acta* **1980**, *44*, 1683–1699.
- (43) Rimstidt, J. D.; Dove, P. M. Mineral/Solution Reaction Rates In A Mixed Flow Reactor: Wollastonite Hydrolysis. *Geochim. Cosmochim. Acta* **1986**, *50*, 2509–2516.
- (44) Stumm, W.; Wollast, R. Coordination Chemistry Of Weathering - Kinetics Of The Surface-Controlled Dissolution Of Oxide Minerals. *Rev. Geophys.* **1990**, *28*, 53–69.
- (45) Ashokkumar, M. The Characterization Of Acoustic Cavitation Bubbles – An Overview. *Ultrason. Sonochem.* **2011**, *18*, 864–872.
- (46) Hänggi, P.; Talkner, P.; Borkovec, M. Reaction-Rate Theory: Fifty Years After Kramers. *Rev. Mod. Phys.* **1990**, *62*, 251–341.
- (47) Toledo-Marín, J. Q.; Naumis, G. G. Short Time Dynamics Determine Glass Forming Ability In A Glass Transition Two-Level Model: A Stochastic Approach Using Kramers' Escape Formula. *J. Chem. Phys.* **2017**, *146*, 094506.
- (48) Yelon, A.; Movaghar, B. Microscopic Explanation Of The Compensation (Meyer-Neldel) Rule. *Phys. Rev. Lett.* **1990**, *65*, 618–620.
- (49) Madon, R. J.; Iglesia, E. Catalytic Reaction Rates In Thermodynamically Non-Ideal Systems. *J. Mol. Catal. A: Chem.* **2000**, *163*, 189–204.
- (50) Walker, T. W.; Chew, A. K.; Li, H.; Demir, B.; Zhang, Z. C.; Huber, G. W.; Van Lehn, R. C.; Dumesic, J. A. Universal Kinetic Solvent Effects In Acid-Catalyzed Reactions Of Biomass-Derived Oxygenates. *Energy Environ. Sci.* **2018**, *11*, 617–628.